

# Quantum computing with trapped ions: a beginner's guide

Francesco Bernardini,<sup>1</sup> Abhijit Chakraborty,<sup>2</sup> and Carlos Ordóñez<sup>3</sup>

<sup>1</sup>*Department of Electrical and Computer Engineering,  
University of Houston, Houston, Texas 77204-4005, USA*

<sup>2</sup>*Institute for Quantum Computing, University of Waterloo, Waterloo, ON, N2L 3G1, Canada*

<sup>3</sup>*Department of Physics, University of Houston, Houston, Texas 77024-5005, USA*

(Dated: March 30, 2023)

This pedagogical article explains the basics of quantum computing using one of the most-used platform for scalable quantum computers: trapped ions. The suitability of the solution is addressed by showing its performance towards DiVincenzo criteria.

## I. INTRODUCTION

Two of the most interesting and promising active fields of research in the last 40 years, quantum computing (QC) and quantum information (QI) have taught us once more that even the hardest problems can significantly simplify, if we find a better way to reformulate them. Until today, indeed, the race to design the smallest chips and build the most powerful supercomputers has based itself on a *classical* model of computing, where binary logic is the underlying language.

But since its inception in the 1970s [1–6], quantum computers have introduced a new language based on the logic of quantum mechanics (QM), providing us with a totally novel way of simulating new problems and designing new algorithms, with the ultimate goal to perform certain tasks faster than their classical counterparts.

Despite being the hotbed of cutting-edge research, the basics of QC and QI is formulated using one of the simplest quantum model, the two-level spin-1/2 system. This has a huge advantage from a didactical viewpoint, as it allows interesting and useful activities to be developed even in an undergraduate environment [8–12].

Nevertheless, QC and QI have potential for application in many diverse areas of physical and social sciences like cryptography (more secure communications procedures using quantum principles), finance (quantum optimization algorithms to guide trading), quantum gravity (simulations of black hole physics using quantum circuits), and urban transportation (methods for intelligent traffic guidance using quantum computers) [13–16] to name a few.

Despite remarkable developments in quantum algorithms and quantum communications theory, the biggest challenge remains to build a scalable quantum computer that can actually perform these tasks. While there have been significant advancements in building a quantum machine lately [17–19], we still are in very early stages of QC. Even the best platform to realise a quantum bit (qubit) is not unanimously agreed upon in the scientific community. However, over the years, trapped ion (TI) systems [20–22] have emerged as one of the most viable QC platform due to its scalability and ease of manipulation over other platforms like nuclei (NMR) [23–25], quantum optical devices [26, 27], superconductors [17, 28]

and quantum dots [29]. Companies like Honeywell and IonQ have already made publicly usable quantum computers using trapped ions, and many research groups across the world also actively use trapped ion platforms for quantum simulations. While IBM has made significant advancement in using the superconducting platform for quantum computing, they are still limited by connectivity issues, making long-range connections between qubits error prone. This is not a problem for trapped ions. However, trapped ion systems suffer from their own disadvantages, which we mention briefly at the end of this article.

There already exists a vast amount of literature and books on trapped ion platforms [30, 33–35], but there is a lack of articles that explain the basics of the quantum computing with emphasis on a physical realization of the system in an undergraduate environment. Scarani [36] in his paper explains nicely the basics of QC but using mostly NMR perspective. In this note, we use a similar pedagogical approach but emphasize on the features of trapped ions system that make them a good candidate for QC, instead of using a purely theoretical viewpoint. In this way, undergraduate students can also have an idea about how quantum computers can be practically realized and manipulated, much like semiconductor devices in classical computers. Connecting the theory with an experimental viewpoint is necessary to get a broader understanding of the physical intricacies and difficulties of building a quantum computer. Such aspects are often lacking in class-friendly literature, and our article aims to bridge this gap.

This article is organized in the following way: Sec. II and III summarizes the theoretical spin-1/2 system. We mention in Sec. IV the qualities that a prospective QC platform must possess for building a successful quantum computer. In Sec. V–X we concisely explain the mechanism of preparing a trapped ion system capable of performing quantum computation and how the laser-ion interaction can be used to change the ionic states. In Sec. XI we describe how the TI system can be manipulated to implement the universal quantum gates, and finally provide some concluding remarks about the performance of the TI system in Sec. XII.

## II. THE QUBIT

Building blocks of QC are called quantum bits (in analogy to the binary digit, or bit, of classical computing), or **qubits**. A qubit is a two-state quantum system where the states are in general eigenvectors of an observable whose physical meaning depends on the platform used to realise the qubit. In Dirac notation, the two states (orthonormal) are denoted by  $|0\rangle$ , and  $|1\rangle$ . A general state of the qubit can be in a superposition of the two states

$$|q\rangle = \cos \frac{\theta}{2} |0\rangle + e^{i\varphi} \sin \frac{\theta}{2} |1\rangle, \quad (1)$$

where  $\theta \in [0, \pi]$  and  $\phi \in [0, 2\pi]$  are two parameters that defines the state. The coefficients of  $|0\rangle, |1\rangle$  determine the probability to obtain the corresponding eigenvalues as a result of a measurement. Due to this probabilistic interpretation, the qubit state has a unit norm (probabilities should add up to one), and the norm is usually preserved in any operation performed on the isolated system. These norm-preserving linear operations are usually called **unitaries**, or **gates** in QC. It can be shown [30] that a generic unitary  $U$  can be generated by suitable exponentials of the Pauli operators  $\sigma_x$ ,  $\sigma_y$ , and  $\sigma_z$ , modulo a phase factor:

$$U = e^{i\alpha} e^{in_j \sigma_j \theta/2} \equiv e^{i\alpha} R_{\hat{n}}(\theta),$$

$$\hat{n} = (n_x, n_y, n_z) \in \mathbb{R}^3, \quad \hat{n} \cdot \hat{n} = 1, \quad (2)$$

where  $R_{\hat{n}}(\theta)$  represents a rotation of angle  $\theta$  around an axis pointed in the direction of  $\hat{n}$ . Pauli operators are Hermitian, traceless, but also unitary so they can be considered as gates themselves. They are defined by their commutation and anticommutation relations:

$$[\sigma_i, \sigma_j] = 2i\epsilon_{ijk}\sigma_k, \quad \{\sigma_i, \sigma_j\} = 2\delta_{ij}. \quad (3)$$

In the following, we will call  $\{|0\rangle, |1\rangle\}$  as the *operational basis* and we will identify it with the set of eigenstates of  $\sigma_z$ :

$$\sigma_z |0\rangle = |0\rangle, \quad \sigma_z |1\rangle = -|1\rangle. \quad (4)$$

The choice of this basis produces a matrix representation for the qubit state and operators:

$$|0\rangle := \begin{pmatrix} 1 \\ 0 \end{pmatrix}, \quad |1\rangle := \begin{pmatrix} 0 \\ 1 \end{pmatrix}, \quad (5)$$

$$\sigma_x := \begin{pmatrix} 0 & 1 \\ 1 & 0 \end{pmatrix}, \quad \sigma_y := \begin{pmatrix} 0 & -i \\ i & 0 \end{pmatrix}, \quad \sigma_z := \begin{pmatrix} 1 & 0 \\ 0 & -1 \end{pmatrix}. \quad (6)$$

## III. MULTIPLE-QUBIT GATES

For a  $N$ -qubit system, the state vector space (Hilbert space) is a tensor product of  $N$  single-qubit space. For

example, a general 2-qubit system can be in a superposition of  $|00\rangle, |01\rangle, |10\rangle, |11\rangle$  vectors. The gates acting on a  $N$ -qubit system are consequently  $2^N \times 2^N$  unitary matrices generated from tensor product of 1-qubit gates. For  $N = 2$ , an important family of gates is represented by the *controlled gates*: according to the state of a *control* qubit, a controlled gate performs a specific action on a *target* qubit. One of the simplest examples is the *CNOT*, or controlled-*NOT*, acting on a pair  $|c\rangle |t\rangle$  where the first qubit represents the control and the second the target:

- If the control qubit is in the  $|0\rangle$  state, *CNOT* does nothing on the target;
- If the control qubit is in the  $|1\rangle$  state, *CNOT* applies  $\sigma_x$  on the target.

The usefulness of this gate lies in the fact that the action of an arbitrary  $N$ -qubit gate can be mimicked with arbitrary accuracy using [7] only 1-qubit rotations  $R_{\hat{n}}(\theta)$  (2) and *CNOT* gates. For this reason, if we can manipulate a physical qubit to perform these two operations, we can in principle perform any other complicated gates.

## IV. REALIZATION OF QUBITS: DIVINCENZO'S CRITERIA

Any physical system whose mathematical description is satisfactorily formulated in terms of a two-level system is a good candidate to represent a qubit. As mentioned in the introduction, nuclei, optical systems, superconducting circuits, quantum dots, and trapped ions are some notable examples. Different platforms have different advantages and disadvantages, and in order to benchmark their fitness for QC applications, DiVincenzo [37] developed five criteria.

1. (a) Qubits must be well characterized and easy to produce. (b) the system must be scalable, i.e. must be able to manage an arbitrary number of qubits;
2. It must be possible to reliably initialize a qubit to a fiducial state, e.g.  $|0\rangle$ ;
3. A qubit must be stable over timescales larger than the typical time needed to operate on it;
4. It must be possible to implement a universal set of quantum gates;
5. A reliable procedure must exist to read out the state of a qubit.

In this paper we will focus on trapped ions, and describe their viability as a QC platform according to these criteria.

## V. ION PRODUCTION

An ion is a nucleus or a molecule whose electron cloud has been deprived (cations) or augmented (anions) by one unit, so the total system is not electrically neutral. Among the several techniques available to (positively) ionize an atom [38–40], we will briefly mention photoionization [41, 42]. It consists of hitting the neutral atom with light tuned to a suitable wavelength, which is capable to excite an outer electron and provide it with enough energy to leave the atomic orbital. Right after ionization, newly created ions are moved into a protected environment that delays electron reabsorption, for a amount of time sufficient to perform all the required experimental activities. However, the particular details of the procedure are not of primary interest to this review and we refer the interested readers to [43, 44] for further reading.

For QC applications, the choice of the element to ionize depends mainly on the atomic structure, and on the ionization energy. Elements belonging to the groups IIA ad IIB of the periodic table:

Be, Mg, Ca, Sr, Ba, Zn, Cd, Hg, Yb

are the most favorable in this sense and are therefore more commonly used.

After ionization, such elements will show a hydrogen-like spectrum of energy states  $|\alpha_i\rangle$ ,  $i \in N$ , characterized by energy levels  $E_{\alpha_i}$ , eigenstates of an atomic Hamiltonian  $H_a$ . Two of these states, which we will call  $|g\rangle$ , *ground*, and  $|e\rangle$ , *excited*, will be singled out and identified with the abstract states  $\{|0\rangle, |1\rangle\}$  of (4).

The transition that links  $|g\rangle$  and  $|e\rangle$  can be chosen either in the optical or in the hyperfine range, and the corresponding qubits are called respectively *optical* and *hyperfine qubits* [21, 22]. See Table I for a succinct comparison between the two. As we can see, the lifetime of the hyperfine qubits are much larger than the optical qubits which usually makes it the preferred choice for QC along with the fact that it is also easier to manipulate.

The current state of the art of ion manipulation techniques [21] allows rates of operation of hundreds of kHz, which means that basic operations over qubits can be performed in times much smaller than the typical lifetimes of optical or hyperfine qubits [45]. Therefore, optical and hyperfine qubits provide a stable, well-characterized, and rapidly manipulable platform, thus satisfying criteria 1a and 3 mentioned in Sec. IV.

## VI. ION TRAPS

What we described so far only concerns the ion's *internal structure*. However, an ion also moves in space, therefore its total Hamiltonian  $H$  will also feature a kinetic and a potential term:

$$H = H_a + \frac{\vec{P}^2}{2M} + V(\vec{x}) \equiv H_a + K + V \quad (7)$$

Properties	Optical qubits	Hyperfine qubits
Range	visible, 380-740 nm, 405-790 THz	microwave, 3-300 mm, 1-100 GHz
Lifetime	$\sim 1$ s	$\sim 10$ min
States	$S$ level and a meta-stable state	Two hyperfine levels.
Example	$6S_{1/2} \equiv  g\rangle$ and $5D_{5/2} \equiv  e\rangle$ levels of $\text{Ba}^+$	$^2S_{1/2}(F = 1, m_F = 0) \equiv  g\rangle$ and $^2S_{1/2}(F = 0, m_F = 0) \equiv  e\rangle$ levels of $\text{Cd}^+$

TABLE I: Typical parameters of the ionic optical and hyperfine transitions used in QC. In the examples  $F, m_F$  represent total angular momentum including the isospin and its  $z$  component.

where  $\vec{P}$  is the momentum,  $M$  is the mass of the ion and  $V(\vec{x})$  is the potential energy the ion is subject to.

A newborn photoionized ion has typically an energy of  $\sim 1$  keV, which corresponds to a speed of  $\sim 1$  m/s for an ion such as  $^{40}\text{Ca}^+$ . At such energies, the ion can be considered a classical system from a motional perspective. So, in order to build a fully quantum system we need to constrain its motion both in range (**trapping**) and speed (**cooling**).

An **ion trap** is a device whose purpose is to keep ions confined within a narrow region of space: necessary condition for this to happen is that the ion feels a **minimum** of the potential energy  $V(\vec{x})$  (the **trap center**) at some point inside the trapping region.

Taking advantage of the charged nature of the ions, a trapping potential can be created using a suitable combination of electric and/or magnetic potentials. Two paradigms exist for the design of such trapping potential:

- The Penning trap [46, 47], where **static** electric **and** magnetic potentials are used;
- The Paul trap [48–51], where **static and oscillating** electric fields are used.

Although both are in principle suitable for QC applications, the Paul trap is currently the most widely used method in academic and industrial environments. A famous theorem due to Earnshaw [68] states that a charged particle cannot find stable equilibrium in a static electric potential that satisfies Laplace equation. However, it is possible to show that in the case of potentials rotating at particular frequencies, solutions of the equations of motion corresponding to a dynamical equilibrium point arise, allowing the charged particle to be confined in a desired volume. A gravitational analogue of a Paul trap can be seen at [69].

Sufficiently close to the trap center, any potential can be well approximated by a quadratic function of the coordinates, i.e., a trapped ion will behave like a **simple harmonic oscillator** (SHO) in 3 dimensions. The most commonly trapping systems used in quantum computing

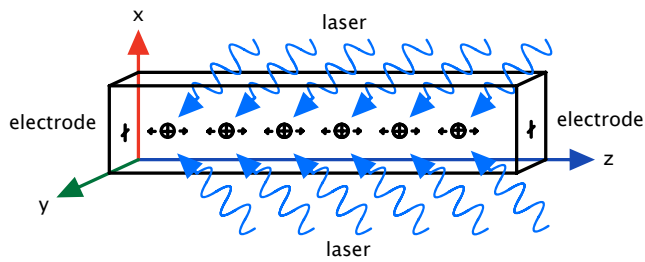


FIG. 1: Ions strongly trapped by a Paul trap in the  $xy$  plane, and allowed to move only in the  $z$  direction. A pair of electrodes prevent the ions from repelling each other out of the trap.

applications are **linear traps**: the trapping force in two of the three dimensions is much stronger than the one in the third (for example, a very strong Paul trap in the  $x$  and  $y$  direction and a relatively weaker pair of electrodes in the  $z$  direction, as in Fig. 1), therefore the only relevant movement will be a simple harmonic motion in (say) the  $\hat{z}$  direction, characterized by a frequency  $\omega_z$  and by the ion's mass  $M$ . Eq. (7) can be recast as

$$H = H_a + \underbrace{\frac{P_z^2}{2M} + \frac{1}{2}M\omega_z^2 z^2}_{H_{SHO}} \equiv H_a + K_z + V_z \quad (8)$$

where  $P_z$  is the momentum in the  $\hat{z}$  direction. Typical experimental values for  $\omega_z$  are in the order of  $\sim 1$  MHz.

In order for the harmonic approximation to hold, the ion must not move appreciably away from the trap center. If this happens, we cannot guarantee anymore that the forces acting on the ion are directed towards the center of the trap, and at some point it could even find itself outside of the trap.

For the above reason it is important that the ion moves slowly, so we want to lower its kinetic energy. With a slight abuse of language we call this stage “cooling” by associating a temperature with the kinetic energy even though the ion is not in thermal equilibrium. In Sec. VII, we will describe two examples of **laser cooling**, valid in the classical and quantum regimes, respectively. Using suitably tuned lasers, it is possible to impart an effective damping force on the ions, which slows them down.

Finally, collisions with other particles are also dangerous as they can induce sudden changes in the kinetic energy. In order to minimize such interactions, an **ultra-high vacuum** [52–54] at pressures of about  $10^{-11}$  Torr ( $\sim 1.3 \times 10^{-9}$  Pa) is created in the region where the trap will be placed.

## VII. LASER COOLING OF IONS

As mentioned in the previous section, we can identify two regimes in cooling depending on how the average oscillator energy  $\langle H_{SHO} \rangle$  compares with the characteristic energy of the quantum SHO (QSHO),  $\hbar\omega_z$ :

- A **classical** regime, where the ion can be considered a classical spring, and quantum phenomena can be neglected. This is a good approximation as long as  $\langle H_{SHO} \rangle$  is much larger than  $\hbar\omega_z$ ;
- A **quantum** regime, where conversely  $\langle H_{SHO} \rangle$  is comparable to  $\hbar\omega_z$ , and quantum effects become important.

Our goal is to bring the ions down to the ground state of the QSHO, which can be used as the fiducial qubit or  $|0\rangle$  on which computation can be performed (criteria 2 in Sec. IV). This is usually a two step process: (a) cooling the system to the point where the vibrational QSHO degrees of freedom (dof) become active, and (b) bringing the QSHO to its ground state. We describe the most used methods to achieve this in the following two subsections.

### A. Classical regime: Doppler cooling

An ion is usually in the classical regime when produced. The primary method used to cool it down to the quantum regime is known as Doppler cooling [55], which uses Doppler shift as the underlying cooling method. As a first step, a resonant transition between two states of the ion is chosen with frequency  $\omega_0$  and linewidth  $\Gamma$ , which represents the width of the absorption maxima in the frequency space.  $\Gamma$  is usually much larger than the QSHO frequency  $\omega_z$ , so that the QSHO levels remain unresolved. These ions are irradiated with a monochromatic laser with frequency tuned to a value slightly lower than the transition frequency:  $\omega_{\text{abs}} = \omega_0 - \delta\omega$  and wave vector  $\vec{k}$  (momentum  $\hbar\vec{k}$ ). Now consider the scattering of an ion moving with velocity  $\vec{v}$  with the laser photon. Suppose that the ion absorbs the photon (the condition of which we will derive shortly), goes to an excited state and then spontaneously decays back by emitting a photon in a random direction with the same energy. For an absorption process, we can write the energy and momentum conservation equation as

$$\hbar\omega_0 + \frac{1}{2}Mv^2 = \hbar\omega_{\text{abs}} + \frac{1}{2}Mv'^2, \quad (9)$$

$$M\vec{v}' = M\vec{v} + \hbar\vec{k}. \quad (10)$$

where  $\vec{v}'$  is the velocity of the ion just after the absorption,  $M$  is the mass of the ion, and the subscript ‘abs’ represents the absorption process. Substituting  $\vec{v}'$  from Eq. (10) into Eq. (9) we get

$$\omega_0 = \omega_{\text{abs}} - \vec{v} \cdot \vec{k} - \frac{\hbar^2 k^2}{2M}. \quad (11)$$

On the RHS, the second term is the well-known Doppler shift, and the third term is known as recoil shift which is usually small compared to the Doppler shift at high velocities. Neglecting the third term and inverting the

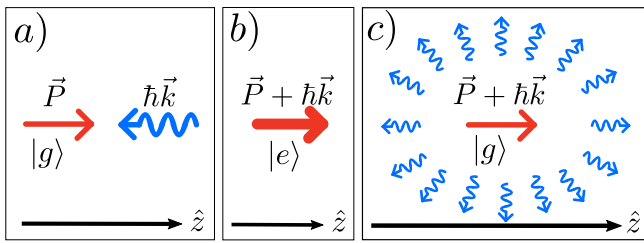


FIG. 2: In the Doppler cooling process, (a) and (b): an ion absorbs a red-shifted laser coming towards it and (c) emits it in a random direction.

expression, we get  $\omega_{\text{abs}} = \omega_0 + \vec{v} \cdot \vec{k}$ . Recalling that the laser frequency was tuned to a value lower than the transition frequency  $\omega_0$ , absorption is only possible if  $\vec{v}$  and  $\vec{k}$  are in opposite direction (making  $\vec{v} \cdot \vec{k}$  negative). So, due to Doppler shift, the ions moving towards the laser absorbs the photon to go to an excited level. Now consider the emission process in which the excited ion emits a photon in a random direction (Fig. 2). Once again from energy and momentum conservation we get

$$\omega_0 = \omega_{\text{em}} - \vec{v}' \cdot \vec{k}_{\text{em}} + \frac{\hbar^2 k^2}{2M}, \quad (12)$$

where the subscript ‘em’ represents emission process and  $|\vec{k}_{\text{em}}| = |\vec{k}|$ . Once again neglecting the recoil shift, we get  $\omega_{\text{em}} = \omega_0 + \vec{v}' \cdot \vec{k}_{\text{em}}$ . But the wave vector of the emitted photon  $\vec{k}_{\text{em}}$  is in a random direction. Hence, averaging over a number of scattering processes we get  $\langle \hbar \vec{v}' \cdot \vec{k}_{\text{em}} \rangle = 0$ . So, on average the energy change of the photon per scattering event is

$$\hbar \Delta \omega = \langle \hbar(\omega_{\text{em}} - \omega_{\text{abs}}) \rangle = -\hbar \vec{v} \cdot \vec{k}. \quad (13)$$

This gain  $\vec{v} \cdot \vec{k}$  in photon energy is equal to the loss of the ion’s kinetic energy ( $E_K$ ), i.e.,  $\Delta E_K = \hbar \vec{v} \cdot \vec{k} < 0$ . If we interpret temperature as  $\frac{3}{2} k_B T = E_K$ , this loss of kinetic energy leads to cooling the ions moving towards the laser.

This process of cooling down ions does not go on indefinitely. One limit to this process can be readily obtained by considering the recoil shift. When the ions have already significantly cooled down, the velocity  $\vec{v}$  is small enough so that the third term in Eq. (11) and (12) cannot be neglected anymore. With the recoil shift incorporated the change in the ions kinetic energy becomes  $\Delta E_K = \hbar \vec{v} \cdot \vec{k} + \hbar^2 k^2 / M$ . This means that the ions will cool down as long as  $\Delta E_K < 0$ , i.e.  $-\hbar \vec{v} \cdot \vec{k} > \hbar^2 k^2 / M$  with  $\vec{v} \cdot \vec{k} < 0$ , imposing a lower limit for the temperature known as the **recoil limit** [56].

### B. Quantum regime: sideband cooling

After Doppler cooling reaches its limit, the energy of the ion is low enough to consider the vibrational degrees

of freedom of the QSHO. Usually, after Doppler cooling, the average QSHO number state of the ion is  $\langle n \rangle \sim 10$ . However, as stated earlier, our goal is to reach the ground state of the harmonic oscillator to initialize the qubit. This requires further cooling of the system, which is generally achieved by a process called **sideband cooling**. For sideband cooling, an internal ionic transition is chosen with linewidth  $\Gamma_s$ , now small compared to  $\omega_z$  (frequency of the QSHO) so that the absorption peak can distinguish frequencies  $\omega_0 \pm \omega_z$  from  $\omega_0$  (as opposed to Doppler cooling where  $\Gamma \gg \omega_z$ ). For this reason, a different transition is chosen from that of the Doppler cooling process. We call the lower and higher level of this transition the internal ground state  $|g\rangle$  and excited state  $|e\rangle$ , respectively and denote this transition frequency as  $\omega_0$ . The free Hamiltonian of the system can be written as

$$H_0 = \hbar \omega_z a^\dagger a + \frac{\hbar}{2} \omega_0 \sigma_z \quad (14)$$

where  $\sigma_z$  is the Pauli spin operator in Eq. (6) corresponding to the two-state ion, and  $a^\dagger, a$  are the raising and lowering operator of the QSHO. Initially the ion is in the state  $|g, n\rangle$  with  $n \sim 10$ . Here, the notation  $|g, n\rangle$  means that the ion is in atomic state  $|g\rangle$  and in QSHO vibrational state  $|n\rangle$ . We want to reach the ground state  $|g, 0\rangle$  to initialize our operational qubit. This is achieved by a repetition of the following transitions  $|g, n\rangle \rightarrow |e, n-1\rangle \rightarrow |g, n-1\rangle$ . This set of transitions are implemented by the interaction of ions with a laser which is considered a classical source of electromagnetic waves. The interaction Hamiltonian is given by

$$H' = \frac{1}{2} \hbar \Omega (\sigma_+ + \sigma_-) \left[ e^{i(kz - \omega t + \phi)} + e^{-i(kz - \omega t + \phi)} \right] \quad (15)$$

where  $k, \omega$  are the wave vector and frequency of the laser, and  $\phi$  is the phase of the laser.  $\Omega$  is the coupling strength,  $\sigma_+, \sigma_-$  are the raising and lowering operator for the internal dof, i.e.,  $\sigma_+ |g\rangle = |e\rangle$ , and  $\sigma_- |e\rangle = |g\rangle$ . Such Hamiltonian is standard in semiclassical description of light-matter interactions [31], and models the simplest type of exchange between an atom and a specific component of frequency  $\omega$  of the electromagnetic field: the usual sinusoidal oscillating factor is represented by the sum  $\frac{1}{2} (e^{i\cdots} + e^{-i\cdots}) \equiv \cos \dots$ .

Note that we have not quantized the electromagnetic waves. However, the position of the atom ( $z$ ) is quantized since  $z = \sqrt{\frac{\hbar}{2M\omega_z}} (a + a^\dagger)$  is determined by the QSHO potential. We define  $\eta = k \sqrt{\frac{\hbar}{2M\omega_z}}$ , a parameter known as the Lamb-Dicke parameter. We now execute the following steps in consecutive order:

- Write  $e^{\pm i\eta(a+a^\dagger)} \approx 1 \pm i\eta(a+a^\dagger)$  as the Lamb-Dicke parameter is usually small in these experiments.
- Go to the interaction picture by substituting  $\sigma_- \rightarrow \sigma_- e^{-i\omega_0 t}$  and its adjoint for  $\sigma_+$ . Use rotating wave

approximation (RWA) to neglect highly oscillating terms where addition of two frequencies  $\omega$  and  $\omega_0$  appears in the phase.

- Finally write interaction picture operators for the

$$H_I = \frac{1}{2}\hbar\Omega \left( \sigma_+ e^{-i(\Delta t - \phi)} + \sigma_- e^{i(\Delta t - \phi)} \right) + \frac{1}{2}\hbar\eta\Omega \left( a\sigma_+ e^{-i(\Delta + \omega_z)t + i\tilde{\phi}} + a^\dagger\sigma_- e^{i(\Delta + \omega_z)t - i\tilde{\phi}} \right) + \frac{1}{2}\hbar\eta\Omega \left( a^\dagger\sigma_+ e^{-i(\Delta - \omega_z)t + i\tilde{\phi}} + a\sigma_- e^{i(\Delta - \omega_z)t - i\tilde{\phi}} \right) \quad (16)$$

where  $\Delta = \omega - \omega_0$ ,  $\tilde{\phi} = \phi + \pi/2$ . The terms in the Hamiltonian are grouped into three contributions. By choosing the laser detuning  $\Delta$ , one can achieve resonance frequency for each one of the three terms and at resonance the other contributions can be ignored. So, there are three different resonance frequencies corresponding to the three terms in the Hamiltonian. In this section, we focus on only one of the resonances. If we choose the detuning as  $\Delta = -\omega_z$ , the second term gives the resonant time independent Hamiltonian

$$H_I^{(\text{rsb})} \approx \frac{1}{2}\hbar\eta\Omega \left( a\sigma_+ e^{i\tilde{\phi}} + a^\dagger\sigma_- e^{-i\tilde{\phi}} \right) \quad (17)$$

The time evolution now becomes straightforward with the time independent interaction Hamiltonian and is given by  $\mathcal{U}_I^{(\text{rsb})}(t) = e^{-iH_I^{(\text{rsb})}t/\hbar}$ . As stated earlier, after the Doppler cooling, the ion is in general in a state  $|g, n\rangle$  with  $n \sim 10$ . Applying the time evolution operator to a such a state  $|g, n\rangle$  yields

$$\mathcal{U}_I^{(\text{rsb})}(t) |g, n\rangle = \cos(\bar{\omega}t) |g, n\rangle - ie^{i\tilde{\phi}} \sin(\bar{\omega}t) |e, n-1\rangle \quad (18)$$

where  $\bar{\omega} = \eta\Omega\sqrt{n}/2$ . The most immediate consequence of (18) is that the final state of the ion can be controlled by timing the application of the evolution operator. For example, by choosing to apply the laser pulse for a time  $t = \pi/\eta\Omega\sqrt{n}$ , the argument of the cosine multiplying the first member becomes  $\frac{\pi}{2}$ , therefore the whole contribution of the state  $|g, n\rangle$  vanishes. The time-evolved state at the end of the interaction process becomes then  $|e, n-1\rangle$  modulo an overall phase. The ion then spontaneously decays from the  $|e, n-1\rangle$  state to  $|g, n-1\rangle$  state. So, at the end of this whole laser-ion interaction the initial state  $|g, n\rangle$  reduces to  $|g, n-1\rangle$ , going one step lower in the QSHO energy level (Fig. 3). Repeating this process multiple times one can reach the ground state of the QSHO with a high accuracy which is now ready for performing computation thus satisfying criteria 2 of Sec. IV.

The particular choice of frequency  $\omega = \omega_0 - \omega_z$  for the laser used for the transition  $|g, n\rangle \rightarrow |e, n-1\rangle$  is known

vibrational dof  $a \rightarrow e^{-i\omega_z t}$ .

After following these steps, the interaction picture Hamiltonian can be written as

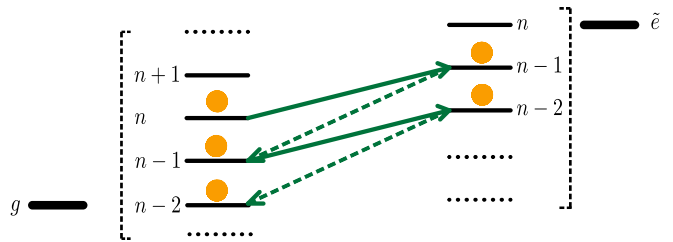


FIG. 3: Schematics of sideband cooling: solid and dashed lines represent, respectively, stimulated absorption and spontaneous emission.

as **red sideband resonance** which reflects in the name of the cooling process.

## VIII. MANIPULATION OF SINGLE IONS

In the previous section, we saw that by choosing the frequency of the laser, we can use the laser-ion interaction to alter the state of the ion. In particular, we showed that the red sideband resonance is used for a transition of the form  $|g, n\rangle \rightarrow |e, n-1\rangle$ . In this section, we introduce two more resonant interactions that are used to manipulate an ion during the quantum computing process:

- **Blue sideband resonance:** From Eq. (16), if the laser detuning is chosen to be  $\Delta = \omega_z$ , the third term in the Hamiltonian prevails due to resonance:

$$H_I^{(\text{bsb})} \approx \frac{1}{2}\hbar\eta\Omega \left( a^\dagger\sigma_+ e^{i\tilde{\phi}} + a\sigma_- e^{-i\tilde{\phi}} \right) \quad (19)$$

The unitary time-evolution operator corresponding to this Hamiltonian induces transitions of the form  $|g, n\rangle \leftrightarrow |e, n+1\rangle$ , which is known as the blue sideband transition.

- **Carrier resonance:** If the frequency of the laser is chosen to be equal to the frequency of the atomic transition  $\omega_0$ , i.e.  $\Delta = 0$ , the resonant Hamiltonian constitutes of the first term in Eq. (16)

$$H_I^{(\text{c})} \approx \frac{1}{2}\hbar\Omega \left( \sigma_+ e^{i\phi} + \sigma_- e^{-i\phi} \right) \quad (20)$$

The time evolution operator in this case does not change the vibrational levels and transitions of the form  $|g, n\rangle \leftrightarrow |e, n\rangle$  takes place, which is known as carrier transition.

Once we have the fiducial qubit  $|g, 0\rangle$  at the end of the cooling process, the three resonant processes can be used to create states spanned by  $\{|g, 0\rangle, |g, 1\rangle, |e, 0\rangle, |e, 1\rangle\}$  since for  $\eta \ll 1$ , it is possible to go only one step up or down in the QSHO energy levels. So, our discussion will be focused on this subspace of the whole available atom-QSHO Hilbert space.

The time-evolution operator corresponding to the three transitions can be written as

$$\mathcal{U}_I = \begin{pmatrix} \cos(\beta/2) & -ie^{-i\tilde{\phi}} \sin(\beta/2) \\ -ie^{i\tilde{\phi}} \sin(\beta/2) & \cos(\beta/2) \end{pmatrix} \quad (21)$$

where  $\beta = \Omega t$  for carrier transition  $\beta = \eta\Omega t$  for the sideband transitions. The phase is  $\phi$  instead of  $\tilde{\phi}$  for carrier transition. Here the basis used to write the matrix for each transition are the two eigenstates that the transition connects

- carrier:  $|g, 0\rangle, |e, 0\rangle$  basis.
- blue sideband:  $|g, 0\rangle, |e, 1\rangle$  basis.
- red sideband:  $|g, 1\rangle, |e, 0\rangle$  basis.

To see how these time-evolution operators are relevant, let us define  $|g, 0\rangle \equiv |0\rangle$ , and  $|e, 0\rangle \equiv |1\rangle$  as the operational basis for QC purposes. We can now use the carrier resonance operator on the state  $|g, 0\rangle$  to get

$$\mathcal{U}_I^{(c)} |g, 0\rangle = \cos(\beta/2) |g, 0\rangle - ie^{i\phi} \sin(\beta/2) |e, 0\rangle \quad (22)$$

We now notice that choosing the laser interaction time  $t = \theta/\Omega$ , and phase  $\phi = \varphi - \pi/2$  produces the general 1-qubit state in Eq. (1). On the other hand, the general 1-qubit state can be thought of as the result of the action of a 1-qubit gate on the fiducial qubit. So, any 1-qubit gate can be applied on the fiducial qubit by using the carrier resonance interaction and by choosing a proper time interval and phase for the laser pulse.

## IX. MANIPULATION OF MULTIPLE IONS

When more than one ion is present in the trap, an additional phenomenon is to be taken into account: electric charges of the same sign repel one another, therefore the trapping potential and the repulsive Coulomb potential between ions will compete to determine the ion density. As is often the case when such competition is present, it is possible to show that an equilibrium state exists: indeed, for linear traps at the usual working temperatures for QC experiments, the motion of ions is quite limited and they tend to form coherent chain-like structures called

**Coulomb crystals** [58]. A full description of the normal modes and the detailed energy levels arising from the study of this structure is outside the scope of the present work, however a thorough treatment of the case of two ions can be found at [70], Par. 11.2.3. We summarize here the results by mentioning that among all its possible collective behaviors, the Coulomb crystal presents a lowest energy one called **center of mass mode**, akin to the motion of a single ion, but now involving the whole chain of trapped particles, moving at unison.

As we have described in sec. VIII, the point of our construction so far has been to exploit the interplay between the vibrational and the atomic degrees of freedom of a single ion. The ions in this crystal can still be considered as individual atomic qubits, but from a motional point of view they have to be regarded, by all means, as a lattice: consequently, they can't anymore change vibrational state individually, and the only allowed energy transitions will necessarily be those associated to the normal modes of the corresponding quantized lattice.

This has two consequences:

- The state of a chain of  $N$  ions must be described as a product of  $N$  individual atomic qubits but just **one global** vibrational qubit:

$$\{|a_1, \nu_1\rangle, \dots, |a_n, \nu_n\rangle\} \rightarrow \{|a_1 \dots a_n, \nu\rangle\}, \quad (23)$$

$$(a_j = g, e, \nu = 0, 1)$$

- Red and blue sideband transitions will now vibrationally affect **the whole chain**, although they still operate on *individual* atomic state of the ions. For example, a red sideband transition applied on the 2nd ion of a two-ion system yields

$$\mathcal{U}_2^{(\text{rsb})}(t) |g_1, g_2, \mathbf{1}\rangle = \cos(\beta/2) |g_1, g_2, \mathbf{1}\rangle - ie^{i\tilde{\phi}} \sin(\beta/2) |g_1, e_2, \mathbf{0}\rangle. \quad (24)$$

It is understood, but it is useful to state explicitly, that the energy exchanged in a vibrational transition of the lattice is now  $N$  times larger than the one formerly involved in single-ion transitions, as  $N$  ions have to change their motion at once.

The fact that the entire lattice is now affected by a vibrational transition implies a sort of long-range interaction between the ions in the crystal. This paves the way for creating entanglement between ions which will be the basis for the implementation of the *CNOT* gate in Sec. XI. Current linear traps can host approximately  $\sim 10^2$  ions, but proposals to scale this solution (to satisfy criterion 1b in Sec. IV) by building trap networks are currently under development: in such setups, photons are used to transfer information between traps [59, 61, 62].

## X. ION READOUT

Once a qubit is prepared, criterion 5 in Sec. IV requires the ability to **reliably** read its status. We know that

we can't have an exhaustive description of a quantum system, as a measurement will inevitably collapse it to an eigenstate of the observable, so we can only adopt a probabilistic approach. A standard way [63] to probe ions involves the selection of an auxiliary excited state  $|e'\rangle$ , well distinct from the ground and excited states  $|g\rangle$  and  $|e\rangle$  within the frequency resolution of the instruments. Also, such state must be **short-lived**, i.e., decay quickly back into  $|g\rangle$ .

The readout procedure then goes as follows: if we shine a laser tuned to the transition  $|g\rangle \rightarrow |e'\rangle$  on an ion, it will absorb photons (and quickly emit them) if the ion qubit has a component in the ground state. The emission is randomly directed and its radiation can be detected by photodetectors (**bright** state).

On the other hand, an ion in the excited state will be transparent to the radiation (**dark** state), and no radiation will be detected by the photodetectors in the whole solid angle. Fig. 4 summarizes these concepts.

Shining the laser on the ion is equivalent to measuring its state. So, we can express the process as the collapse of a target state

$$|\Psi\rangle = \alpha_{\text{bright}} |g\rangle + \alpha_{\text{dark}} |e\rangle \quad (25)$$

to either the ground, or the excited state, with probabilities  $P_{\text{bright}} = |\alpha_{\text{bright}}|^2$  and  $P_{\text{dark}} = |\alpha_{\text{dark}}|^2$ . In order to estimate  $P_{\text{bright}}$  and  $P_{\text{dark}}$ , it is necessary to repeat the preparation and the measurement of the state a sufficiently large number of times. The aforementioned techniques can reach levels of precision of 99.99% and above [64].

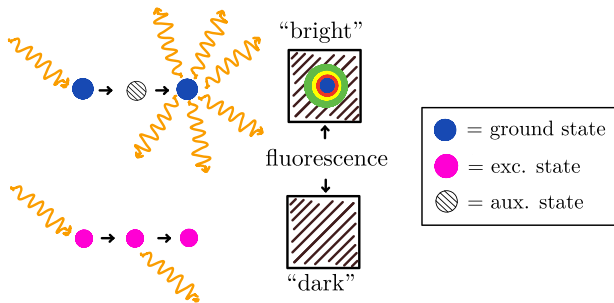


FIG. 4: Readout of ions: ions interacting with the laser will either fluoresce (if they are in the ground state) or remain inert (if they are in the excited state). The emitted radiation is collected by the photodetector and will result in a bright spot on the detector surface.

## XI. QUANTUM COMPUTING WITH TRAPPED IONS

We have showed that a TI system can be accurately prepared in a fiducial state, is scalable, can be manipulated using laser-ion interaction, and the final state can be read out effectively. We also showed that we can apply

any 1-qubit gate to the initial state by using a laser pulse with a fixed phase, duration, and carrier transition frequency. However, it still remains to be seen if we can create any multiple qubit gate on the system. As discussed in Sec. III, any multiple qubit gate can be obtained using 1-qubit gates and a 2-qubit CNOT gate. So, in this section we discuss the process to implement the CNOT gate. As we will show shortly, a CNOT gate can be built using **Hadamard gate** and **Controlled-Z** gates. So, we will first discuss how to implement these two building blocks below. As before, we define  $|g, 0\rangle \equiv |0\rangle$ , and  $|e, 0\rangle \equiv |1\rangle$  as the operational basis [65]. While both the atomic state and the vibrational states can be used as separate qubits, usually the vibrational qubits are only considered as auxiliary qubits (for intermediate computation), not as measurable qubits because they are hard to measure.

### A. Hadamard gate

The Hadamard gate is the unitary operation defined by its action on the operational basis:

$$H|0\rangle = \frac{|0\rangle + |1\rangle}{\sqrt{2}}, \quad H|1\rangle = \frac{|0\rangle - |1\rangle}{\sqrt{2}} \quad (26)$$

so that in the  $\{|0\rangle, |1\rangle\}$  basis the gate is represented by

$$H = \frac{1}{\sqrt{2}} \begin{pmatrix} 1 & 1 \\ 1 & -1 \end{pmatrix} \quad (27)$$

Using Eq. (21) for the carrier transition, we can check that if we use a laser pulse with  $\beta = \frac{\pi}{2}$  and  $\phi = -\pi/2$  followed by a laser pulse with  $\beta = \pi$  and  $\phi = \pi$ , we get Eq. (27) upto an overall phase.

### B. Controlled-Z gate

The controlled-Z (CZ) gate is a **two-qubit gate** which performs a task on a target qubit depending on the control qubit - much like a CNOT gate. Its action can be described as:

- does nothing to the target qubit if the control qubit is  $|0\rangle$ ,
- changes the phase of the target qubit by  $\pi$  (or equivalently flips the sign) if the control qubit is  $|1\rangle$ .

Since this is a two-qubit gate, we need two labels for the atomic dofs of the ions. The basis for the two-qubit Hilbert space is then  $\{|gg, 0\rangle, |ge, 0\rangle, |eg, 0\rangle, |ee, 0\rangle\}$  where the first label denotes the first ion (also the control qubit) and the second label denotes the second ion (target ion). Dropping the vibrational label for convenience

the CZ gate can be expressed as

$$CZ := \begin{pmatrix} |gg\rangle & |ge\rangle & |eg\rangle & |ee\rangle \\ 1 & 0 & 0 & 0 \\ 0 & 1 & 0 & 0 \\ 0 & 0 & 1 & 0 \\ 0 & 0 & 0 & -1 \end{pmatrix} \begin{matrix} |gg\rangle \\ |ge\rangle \\ |eg\rangle \\ |ee\rangle \end{matrix} \quad (28)$$

To implement the CZ gate we need to construct two more one-ion gates that are described below.

**Swap gate between atomic and vibrational states (SWAP<sub>av</sub>):** In this case we consider both atomic and vibrational state of one ion and the basis for this space is  $\{|g, 0\rangle, |g, 1\rangle, |e, 0\rangle, |e, 1\rangle\}$ . The action of the SWAP<sub>av</sub> gate is represented by the matrix

$$\text{SWAP}_{av} := \begin{pmatrix} |g, 0\rangle & |g, 1\rangle & |e, 0\rangle & |e, 1\rangle \\ 1 & 0 & 0 & 0 \\ 0 & 0 & 1 & 0 \\ 0 & -1 & 0 & 0 \\ 0 & 0 & 0 & 1 \end{pmatrix} \begin{matrix} |g, 0\rangle \\ |g, 1\rangle \\ |e, 0\rangle \\ |e, 1\rangle \end{matrix} \quad (29)$$

with the only non-trivial actions given by  $|g, 1\rangle \rightarrow -|e, 0\rangle$ , and  $|e, 0\rangle \rightarrow |g, 1\rangle$ . This can be achieved by the laser detuned to red sideband. Using Eq. (21) for red sideband transition (using the  $\{|g, 1\rangle, |e, 0\rangle\}$  basis) the SWAP<sub>av</sub> gate can be performed by choosing laser pulse with  $\beta = \pi$  and  $\tilde{\phi} = 3\pi/2$ . The inverse of the swap gate can be implemented by changing the phase of the laser to  $\tilde{\phi} = \pi/2$ .

**CZ gate between atomic and vibrational states (CZ<sub>av</sub>):** This is a controlled Z gate acting on the atomic and vibrational states of a single ion where the atomic state acts as the control and the vibrational state acts as the target state. In the single-ion basis  $\{|g, 0\rangle, |g, 1\rangle, |e, 0\rangle, |e, 1\rangle\}$  the gate is represented by

$$CZ_{av} := \begin{pmatrix} |g, 0\rangle & |g, 1\rangle & |e, 0\rangle & |e, 1\rangle \\ 1 & 0 & 0 & 0 \\ 0 & 1 & 0 & 0 \\ 0 & 0 & 1 & 0 \\ 0 & 0 & 0 & -1 \end{pmatrix} \begin{matrix} |g, 0\rangle \\ |g, 1\rangle \\ |e, 0\rangle \\ |e, 1\rangle \end{matrix} \quad (30)$$

with the nontrivial action  $|e, 1\rangle \rightarrow -|e, 1\rangle$ . To implement this gate an auxiliary level  $|\tilde{e}, 0\rangle$  of the ion is found which can be reached only from the  $|e, 1\rangle$  state by means of a laser tuned to  $\omega_{\tilde{e}e} + \omega_z$  (Fig. 5). This is a blue sideband transition in the  $\{|\tilde{e}, 0\rangle, |e, 1\rangle\}$  basis with the former being the lower energy state replacing  $|g, 0\rangle$  in the usual description. Using Eq. (21) for the blue sideband resonance with this basis it is easy to check that if we choose  $\beta = 2\pi$ , we get  $|e, 1\rangle \rightarrow -|e, 1\rangle$ . Since we are using an auxiliary level for the transition, the other original states are left unchanged, giving the only nontrivial change in (30).

Now we are ready to implement the CZ gate for two ions. The most generic state for the two-ion system with

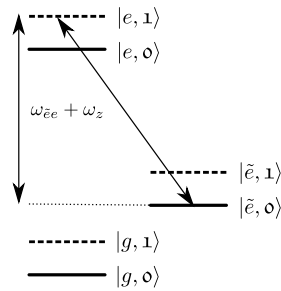


FIG. 5: Auxiliary level used for the implementation of the CZ (same ion).

the vibrational dof in ground state is given by

$$|\Psi\rangle = \alpha |gg, 0\rangle + \beta |ge, 0\rangle + \gamma |eg, 0\rangle + \delta |ee, 0\rangle. \quad (31)$$

The procedure to implement CZ gate is (here and in the next steps, the boldface highlights the qubits that actually change):

- Use the SWAP<sub>av</sub> gate on the second ion:

$$\alpha |gg, 0\rangle + \beta |gg, \mathbf{1}\rangle + \gamma |eg, 0\rangle + \delta |eg, \mathbf{1}\rangle. \quad (32)$$

- Apply a CZ<sub>av</sub> to the first ion:

$$\alpha |gg, 0\rangle + \beta |gg, \mathbf{1}\rangle + \gamma |eg, 0\rangle - \delta |eg, \mathbf{1}\rangle. \quad (33)$$

- Use the inverse of the SWAP<sub>av</sub> gate on the second ion:

$$\alpha |gg, 0\rangle + \beta |ge, \mathbf{0}\rangle + \gamma |eg, 0\rangle - \delta |ee, \mathbf{0}\rangle. \quad (34)$$

### C. CNOT gate

We are finally ready to implement the CNOT gate by applying the following gates in order

$$CNOT := (\mathbb{I} \otimes H) CZ (\mathbb{I} \otimes H), \quad (35)$$

where the gates are applied from right to left.  $\mathbb{I} \otimes H$  here means that the first ion is left unchanged (hence the identity operation) and the second ion is acted on by the Hadamard gate. By writing down the matrix representations, it can be easily checked that Eq. (35) yields the matrix representation of the two-ion CNOT gate

$$CNOT := \begin{pmatrix} |gg\rangle & |ge\rangle & |eg\rangle & |ee\rangle \\ 1 & 0 & 0 & 0 \\ 0 & 1 & 0 & 0 \\ 0 & 0 & 0 & 1 \\ 0 & 0 & 1 & 0 \end{pmatrix} \begin{matrix} |gg\rangle \\ |ge\rangle \\ |eg\rangle \\ |ee\rangle \end{matrix} \quad (36)$$

The first CNOT gate was realized [60] in 1995 by Monroe et al. using the atomic and vibrational degrees of freedom of a Beryllium ion.

## D. Entanglement production

The ultimate advantage of quantum computation lies in using the power of entangled qubits (highly correlated qubits). As a last step, to demonstrate that the TI system is a potent QC platform, we show that indeed one can create entangled ions which we can use to perform quantum algorithms in the lab. By applying the operation  $CNOT(H \otimes \mathbb{I})$  on the two-ion ground state one can create the maximally entangled Bell state  $|\Phi^+\rangle$

$$\begin{aligned} CNOT(H \otimes \mathbb{I})|gg\rangle &= CNOT \frac{|gg\rangle + |eg\rangle}{\sqrt{2}} \\ &= \frac{|gg\rangle + |ee\rangle}{\sqrt{2}} \equiv |\Phi^+\rangle. \end{aligned} \quad (37)$$

## XII. CONCLUDING REMARKS

Throughout the article, we have shown that trapped ion systems satisfy the Di Vincenzo criteria satisfactorily for them to be used as a platform for quantum computing. In short,

1. *Criteria 1(a) and 2:* Trapped ion qubits are robust and can be initialized to high accuracy.
2. *Criteria 3:* The ions have a high coherence time ( $\sim 10^1$  s) to gate time ( $\sim 10^{-6}$  s) ratio, giving enough time to perform computation on the system before effects of decoherence creeps in.
3. *Criteria 4 and 5:* It is possible to implement a universal set of gates and read individual ions by carefully tuning the laser pulses.

Apart from that, as trapped ions are manipulated by laser pulses, ions physically far away from each other can be entangled easily, which is a challenge for superconducting qubits. This makes trapped ions a preferable platform to simulate long-range interactions, which are very common in quantum many body physics and high

energy physics.

However, as with other platforms, scalability (Criteria 1(b)) remains a big issue for trapped ions. In fact, many of the Di Vincenzo criteria breaks down when the ion chain contains multiple ions. The main difficulties are:

1. *Coherence time:* Larger ion chains have shorter coherence time. The effects of decoherence are much larger in chains of length  $\sim 100$  ions.
2. *Readout:* With long chain, it becomes harder to readout individual ions with a high accuracy because the accuracy needed for the parameters of laser pulses to measure individual ions goes beyond what current technology can achieve.

Apart from difficulties due to scalability, the absolute gate time for trapped ions is large ( $\sim 10^{-6}$  s) compared to that of superconducting qubits ( $10^{-9}$  s). So, performing the same computation on a trapped ion platform will take much longer time and poses a challenge to achieve quantum supremacy.

Although it seems that these problems are insurmountable, physicists are continuously developing more ingenious ways to deal with these issues. For a recent and comprehensive review, we encourage readers to take a look at Ref. [66]. While the problem of scalability and decoherence still remains largely unresolved, this is what makes this field all the more interesting and challenging. Until these issues are resolved, we remain in the era of noisy intermediate-scale quantum era (NISQ) devices, and it is hard to predict which platform will emerge victorious in the long run, if at all. Nevertheless, physicists have already been able to use NISQ era devices to simulate physical problems and provide proof-of-concept implementations [67], and we look forward to more developments in the near future.

- 
- [1] R. P. Feynman, Simulating physics with computers, Int. J. Theor. Phys, 21(6/7). (1982)
- [2] R. P. Feynman, Feynman lectures on computation, CRC Press. (2018)
- [3] J. L. Park, The concept of transition in quantum mechanics, Foundations of Physics, 1(1), 23-33. (1970)
- [4] C. H. Bennett, Logical reversibility of computation, IBM journal of Research and Development, 17(6), 525-532. (1973)
- [5] R. S. Ingarden, Quantum information theory, Reports on Mathematical Physics, 10(1), 43-72. (1976)
- [6] D. Deutsch, Quantum theory, the Church-Turing principle and the universal quantum computer, Proceedings of the Royal Society of London. A. Mathematical and Physical Sciences, 400(1818), 97-117. (1985)
- [7] Kitaev, A. Yu. Quantum computations: algorithms and error correction. Russian Mathematical Surveys 52.6 (1997): 1191.
- [8] D. Dehlinger and M. W. Mitchell, Entangled photons, nonlocality, and Bell inequalities in the undergraduate laboratory, American Journal of Physics 70, 903 (2002)
- [9] D. Candela, Undergraduate computational physics projects on quantum computing, American Journal of Physics, 83(8), 688-702. (2015)
- [10] F. W. Strauch, Resource letter QI-1: Quantum information, American Journal of Physics, 84(7), 495-507. (2016)
- [11] M. N. Beck and M. Beck, Witnessing entanglement in an undergraduate laboratory, American Journal of Physics,

- 84(2), 87-94. (2016)
- [12] J. Rodríguez-Laguna and S. N. Santalla, Building an adiabatic quantum computer simulation in the classroom, *American Journal of Physics*, 86(5), 360-367. (2018)
- [13] E. Gerjuoy, Shor's factoring algorithm and modern cryptography. An illustration of the capabilities inherent in quantum computers, *American journal of physics*, 73(6), 521-540. (2005)
- [14] S. Orus, S. Muel and E. Lizaso, Quantum computing for finance: overview and prospects, *Reviews in Physics*, 4, 100028. (2019)
- [15] K. A. Landsman *et al.*, Verified quantum information scrambling, *Nature*, 567(7746), 61-65. (2019)
- [16] S. Feld *et al.*, A hybrid solution method for the capacitated vehicle routing problem using a quantum annealer, *Frontiers in ICT*, 6, 13. (2019)
- [17] F. Arute *et al.*, Quantum supremacy using a programmable superconducting processor, *Nature*, 574(7779), 505-510. (2019)
- [18] Google AI Quantum, Hartree-Fock on a superconducting qubit quantum computer, *Science*, 369(6507), 1084-1089. (2020)
- [19] M. Mohseni *et al.*, Commercialize quantum technologies in five years, *Nature*, 543(7644), 171-174. (2017)
- [20] J. I. Cirac and P. Zoller, Quantum computations with cold trapped ions, *Physical review letters*, 74(20), 4091. (1995)
- [21] B. B. Blinov *et al.*, Quantum computing with trapped ion hyperfine qubits. *Quantum Information Processing* 3.1 (2004): 45-59.
- [22] M. R. Dietrich *et al.*, Hyperfine and optical barium ion qubits. *Physical Review A* 81.5 (2010): 052328.
- [23] T. D. Ladd *et al.*, Quantum computers, *Nature*, 464(7285), 45-53. (2010)
- [24] I. L. Chuang *et al.*, Bulk quantum computation with nuclear magnetic resonance: theory and experiment, *Proceedings of the Royal Society of London. Series A: Mathematical, Physical and Engineering Sciences*, 454(1969), 447-467. (1998)
- [25] T. Xin *et al.*, Nuclear magnetic resonance for quantum computing: techniques and recent achievements, *Chinese Physics B*, 27(2), 020308. (2018)
- [26] T. Pellizzari *et al.*, Decoherence, continuous observation, and quantum computing: A cavity QED model, *Physical Review Letters*, 75(21), 3788. (1995)
- [27] X. Qiang *et al.*, Large-scale silicon quantum photonics implementing arbitrary two-qubit processing, *Nature photonics*, 12(9), 534-539. (2018)
- [28] L. H. Huang, D. Wu, D. Fan, and X. Zhu, Superconducting quantum computing: a review, *Science China Information Sciences*, 63(8), 1-32. (2020)
- [29] D. Loss, and D. P. DiVincenzo, Quantum computation with quantum dots, *Physical Review A*, 57(1), 120. (1998)
- [30] M. A. Nielsen and I. L. Chuang, *Quantum computation and quantum information*, 10<sup>th</sup> Anniversary Edition, Cambridge University Press. (2010)
- [31] H. Haken, *Laser theory. Light and Matter Ic/Licht und Materie Ic*. Springer, Berlin, Heidelberg, 1970. 1-304.
- [32] M. Le Bellac. A short introduction to quantum information and quantum computation. Cambridge University Press, 2006.
- [33] C. D. Bruzewicz, J. Chiaverini, R. McConnell, and J. M. Sage, Trapped-ion quantum computing: Progress and challenges, *Applied Physics Reviews*, 6(2), 021314. (2019)
- [34] D. Esteve, J. M. Raimond, and J. Dalibard, Quantum entanglement and information processing: lecture notes of the Les Houches Summer School 2003. Elsevier. (2004)
- [35] H. Häffner, C. F. Roos, and R. Blatt, Quantum computing with trapped ions. *Physics reports*, 469(4), 155-203. (2008)
- [36] V. Scarani, Quantum computing, *American Journal of Physics*, 66, 956 (1998)
- [37] D. P. DiVincenzo, The physical implementation of quantum computation, *Fortschritte der Physik: Progress of Physics*, 48, 771-783 (2000).
- [38] C. Barshick, D. Duckworth and D. Smith (Eds.), *Inorganic mass spectrometry: fundamentals and applications*, CRC Press. (2000)
- [39] T. D. Märk and G. H. Dunn (Eds.), *Electron impact ionization*, Springer Science & Business Media. (2013)
- [40] A. G. Harrison, *Chemical ionization mass spectrometry*, CRC press. (1992)
- [41] W. E. Cooke, "Ionization of atoms by electric fields," *American Journal of Physics*, 60(8), 757-759. (1992)
- [42] V. Letokhov, "Laser photoionization spectroscopy," Elsevier. (2012)
- [43] L. Deslauriers *et al.*, "Efficient photoionization loading of trapped ions with ultrafast pulses," *Physical Review A*, 74(6), 063421. (2006)
- [44] D. M. Lucas *et al.*, "Isotope-selective photoionization for calcium ion trapping," *Physical Review A*, 69(1), 012711. (2004)
- [45] R. Ozeri, "The trapped-ion qubit tool box," *Contemporary Physics*, 52(6), 531-550. (2011)
- [46] L. S. Brown and G. Gabrielse, "Geonium theory: Physics of a single electron or ion in a Penning trap," *Reviews of Modern Physics*, 58(1), 233. (1986)
- [47] H. Dehmelt, "A single atomic particle forever floating at rest in free space: New value for electron radius," *Physica Scripta*, 1988(T22), 102. (1988)
- [48] W. Paul and H. Steinwedel, "Ein neues massenspektrometer ohne magnetfeld," *Zeitschrift für Naturforschung A*, 8(7), 448-450. (1953)
- [49] W. Paul, "Electromagnetic traps for charged and neutral particles," *Reviews of modern physics*, 62(3), 531. (1990)
- [50] L. Ruby, "Applications of the Mathieu equation," *American Journal of Physics*, 64(1), 39-44. (1996)
- [51] W. Rueckner, "Rotating Saddle Paul Trap," *American Journal of Physics*, 63(2), 186-87. (1995)
- [52] B. R. F. Kendall and D. R. David, "High-Vacuum System for Teaching and Research," *American Journal of Physics*, 36(3), 234-239. (1968)
- [53] D. Hoffman, B. Singh and J. H. Thomas III, *Handbook of vacuum science and technology*, Elsevier. (1997)
- [54] P. K. Naik, *Vacuum: Science, Technology and Applications*, CRC Press. (2018)
- [55] D. J. Wineland, and W. M. Itano, Laser cooling of atoms, *Physical Review A*, 20(4), 1521. (1979)
- [56] The recoil limit is usually less than the Doppler limit which arises due to the non-zero linewidth of the absorption maxima. The Doppler limit takes place when the Doppler shift  $\vec{v} \cdot \vec{k}$  becomes comparable to  $\Gamma$  and in most cases provides the lowest temperature achievable by Doppler cooling. For more details see Ref. [55].
- [57] This small Lamb-Dicke parameter regime has another interpretation. We notice that  $\eta^2 = \frac{\hbar^2 k^2 / 2M}{\hbar \omega_z}$ , which is the

ratio of the recoil energy and the QSHO transition energy. For  $\eta \ll 1$ , the recoil energy is small compared to the transition energy which ensures that spontaneous emission occurs only between levels  $|e, n\rangle \rightarrow |g, n\rangle$ , i.e. at carrier frequency.

- [58] R. C. Thompson, Ion coulomb crystals, *Contemporary Physics*, 56(1), 63-79. (2015)
- [59] C. Monroe *et al.*, Large-scale modular quantum-computer architecture with atomic memory and photonic interconnects, *Physical Review A*, 89(2), 022317. (2014)
- [60] C. Monroe *et al.*, Demonstration of a fundamental quantum logic gate. *Physical review letters* 75.25 (1995): 4714.
- [61] D. Hucul *et al.*, Modular entanglement of atomic qubits using photons and phonons, *Nature Physics*, 11(1), 37-42. (2015)
- [62] I. V. Inleket *et al.*, Multispecies trapped-ion node for quantum networking, *Physical review letters*, 118(25), 250502. (2017)
- [63] D. C. Marinescu, *Classical and quantum information*, Academic Press. (2011)
- [64] A. H. Burrell, *High fidelity readout of trapped ion qubits*, (Doctoral dissertation, Oxford University, UK). (2010)
- [65] In principle, red- and blue-sideband transitions allows jumps between the pairs of states  $|g, 1\rangle \leftrightarrow |e, 0\rangle$  and  $|g, 0\rangle \leftrightarrow |e, 1\rangle$ . From a structural standpoint, such pairs are in no way inferior to  $\{|g, 0\rangle, |e, 0\rangle\}$ . However, we did not consider them as the operational basis of the qubits because the time needed to induce a flip between a  $\{|g, 1\rangle, |e, 0\rangle\}$  or a  $\{|g, 0\rangle, |e, 1\rangle\}$  pair in a red/blue sideband transition is **much larger** than in the case of a  $\{|g, 0\rangle, |e, 0\rangle\}$  in a carrier transition. This would make any prospective quantum computer much slower.
- [66] C. D. Bruzewicz, J. Chiaverini, R. McConnell, and J. M. Sage, Trapped-ion quantum computing: Progress and challenges, *Applied Physics Reviews*, 6(2), 021314. (2019)
- [67] J. Preskill, Quantum computing in the NISQ era and beyond, *Quantum*, 2, 79. (2018)
- [68] S. Earnshaw, *Trans. Cambridge Philos. Soc.*, 7 (1842), p. 97
- [69] "Paul trap", UCLA Physics video <https://www.youtube.com/watch?v=Xb-zpMOU0zk>
- [70] Sagawa, H., Yoshida, N., *Fundamentals of quantum information* (2011).